Structural, Optical, and Electrical Properties of Self-Assembled Films of PbSe Nanocrystals Treated with 1,2-Ethanedithiol

Joseph M. Luther,[†,‡,§] Matt Law,[†,§] Qing Song,[†] Craig L. Perkins,[†] Matthew C. Beard,[†] and Arthur J. Nozik[†,*]

[†]National Renewable Energy Laboratory, Golden, Colorado 80401, and [‡]Department of Physics, Colorado School of Mines, Golden, Colorado 80401. [§]These authors contributed equally to this work.

ABSTRACT We describe the structural, optical, and electrical properties of high-quality films of PbSe nanocrystals fabricated by a layer-by-layer (LbL) dip-coating method that utilizes 1,2-ethanedithiol (EDT) as an insolubilizing agent. Comparative characterization of nanocrystal films made by spin-coating and by the LbL process shows that EDT quantitatively displaces oleic acid on the PbSe surface, causing a large volume loss that electronically couples the nanocrystals while severely degrading their positional and crystallographic order of the films. Field-effect transistors based on EDT-treated films are moderately conductive and ambipolar in the dark, becoming *p*-type and 30 – 60 times more conductive under 300 mW cm^{-2} broadband illumination. The nanocrystal films oxidize rapidly in air to yield, after short air exposures, highly conductive *p*-type solids. The LbL process described here is a general strategy for producing uniform, conductive nanocrystal films for applications in optoelectronics and solar energy conversion.

KEYWORDS: nanocrystals · PbSe · multiple exciton generation · films · 1,2-ethanedithiol · field-effect transistor · oxidation

Thin films of semiconductor nanocrystals (NCs) are emerging as an important class of materials for electronic and optoelectronic devices such as field-effect transistors,[1–7] photodetectors,[8–11] light-emitting diodes,[12–16] metamaterials,[17–19] and solar cells.[20,21] The discovery of efficient multiple exciton generation (MEG) by single photons in lead chalcogenide NCs[22,23] and in films of electronically coupled NCs[24] has initiated an intense effort to build NC photovoltaic devices that exhibit external quantum efficiencies substantially greater than 100% at wavelengths relevant to solar energy conversion. Calculations show that solar cells utilizing single MEG absorbers can be up to 44% efficient at one sun, compared to ~33% for cells utilizing conventional absorbers.[25] The potential for high device efficiency and inexpensive fabrication drives the development of NC solar cells.

Here we describe the structural, optical, and electrical properties of uniform and conductive films of PbSe NCs fabricated by a layer-by-layer (LbL) dip-coating method. In this method, a monolayer of NCs is deposited on a substrate by dip-coating and then washed in 1,2-ethanedithiol (EDT) in acetonitrile to remove the electrically insulating oleic acid molecules that originally solubilize the NCs. Large-area, crack-free NC films are readily produced by repeating this procedure until the desired film thickness is attained. We have recently used these films to construct NC solar cells exhibiting large short-circuit current densities (>24 mA cm^{-2}).[26] In order to improve these devices, we seek a basic understanding of the properties of the EDT-treated LbL PbSe NC films.

RESULTS AND DISCUSSION

Spin-Cast NC Films. To elucidate the effect of the EDT treatment on PbSe NC solids, we first prepared a series of 450-nm-thick films by spin-coating a 380 mg mL^{-1} solution of NCs in octane onto various substrates. Spin-coating yields NC superlattices characterized by strong PbSe 220 texture in wide-angle X-ray scattering (WAXS) patterns and multiple sharp reflections in small-angle X-ray scattering (SAXS) patterns, similar to films made by Talapin and Murray by drop-casting.[4] As-made NC films were compared with films treated in EDT using Fourier transform infrared (FTIR) spectroscopy, WAXS and SAXS, X-ray photoelectron spectroscopy (XPS), optical absorption spectroscopy, and scanning electron microscopy (SEM).

Soaking spin-cast NC films in 0.1 M EDT in acetonitrile for several minutes

*Address correspondence to arthur_nozik@nrel.gov.

Received for review October 29, 2007 and accepted January 11, 2008.

Published online January 31, 2008.
10.1021/nn7003348 CCC: $40.75

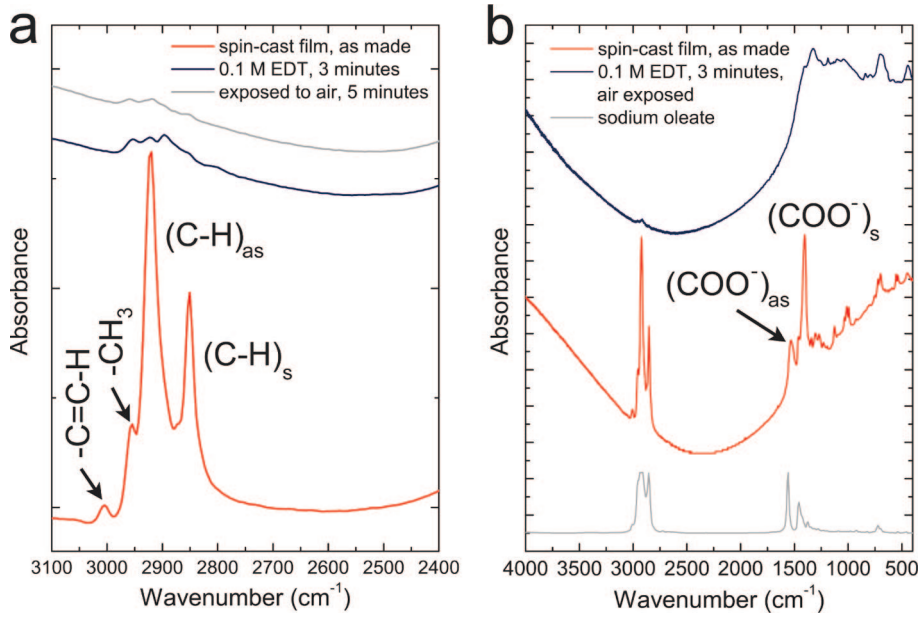

Figure 1. FTIR spectra of 450-nm-thick spin-cast PbSe NC films before and after EDT treatment. (a) The C−H and S−H stretch region. Treated films retain 12–14% of the C−H intensity of untreated films. Quantitative exchange of oleate by EDT would be expected to lower the C−H intensity to approximately 12% of its original intensity (4 C−H bonds in EDT *versus* 33 C−H bonds in oleic acid). Exposing treated films to air for 5 min results in a further 3−6-fold loss of C−H intensity because of desorption of EDT (see the section on film oxidation in the text). Note the absence of S−H signal at ~2550 cm^{-1} in the spectrum of the treated films. (b) Survey spectra, acquired in air. The treated, air-exposed film retains only 2% of the C−H signal of the untreated film. Spectra of the as-made PbSe films are very similar to those of oleate-capped cobalt NCs made by Wu *et al.*[30] At the bottom is a sodium oleate spectrum for reference. See Figure S5 for reference spectra of EDT and ethanethiol.

quantitatively removes oleate from the surface of the nanocrystals (Figure 1).[29] This reaction probably occurs *via* the nucleophilic attack of oleate by EDT, followed by Pb−S bond formation and desorption of oleic acid, or by the dissociative adsorption of EDT on the NC surface to yield adsorbed $HS(CH_2)_2S^-$ and hydrogen, again followed by desorption of oleic acid (see Figure S3). As a result of oleate removal, the NCs move closer together, the NC superlattice becomes disordered, and the films crack extensively (Figure 2). WAXS shows that the NC size is unchanged by the EDT treatment (Figure 3). A decrease in the intensity of the PbSe 220 peak in WAXS patterns indicates that the NCs tilt and rotate as the layers of NCs within the film buckle from the loss of oleate. We estimate that oleate accounts for 30–40% of the original film volume.

The surface coverage of EDT is fairly high on EDT-treated films that are protected from air. XPS shows substantial sulfur at the film surface after exposure to EDT (Figure 4), and the C−H stretch signal in the FTIR spectra is as strong as expected for quantitative replacement of oleate with EDT (Figure 1). The absence of the S−H stretch at ~2550 cm^{-1} suggests that adsorbed EDT exists as ethanedithiolate[31,32] bound in a bidentate fashion either on single NCs or between NCs. Furthermore, the sulfur $2p_{3/2}$ X-ray photoelectron peak at 161.5 eV is characteristic of bound thiolate rather than the free C−S−H moiety.[33] XPS depth profiles measure sulfur in the film at a concentration of 3.3 ± 0.35 atom % (Figure S6). The relatively high coverage of EDT implies that the PbSe NC films might have a low density of unpassivated surface states. However, our electrical measurements, discussed below, show that carrier traps dominate the electrical behavior of the films.

Removal of the insulating oleate and the concomitant decrease in the nanocrystal spacing triggers a Mott-type insulator-to-conductor transition[34] that has a marked effect on the optical absorption of the spin-cast films. Figure 5 shows that the EDT treatment causes the first excitonic transition of the nanocrystals to red-shift by 86 nm (27 meV). At the same time, absorbance is enhanced across most of the spectrum such that the film color changes from a translucent brown, character-

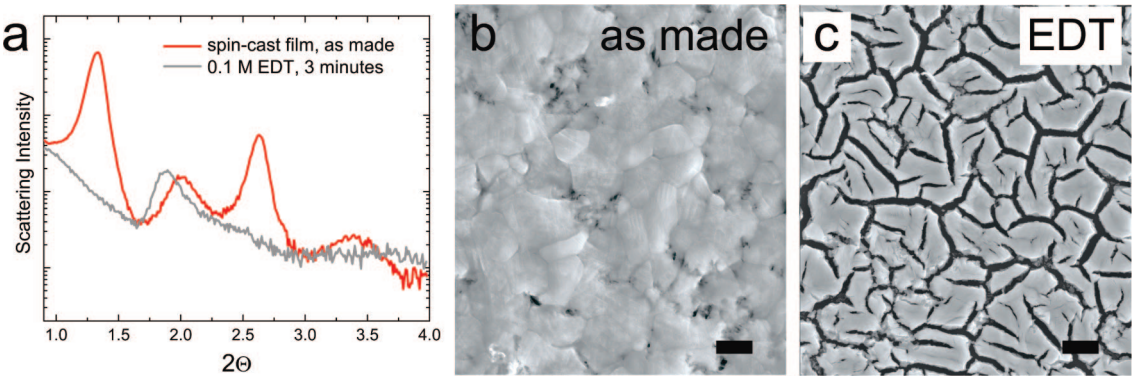

Figure 2. Microstructure of the spin-cast NC films before and after EDT treatment. (a) SAXS data, showing a ~16 Å decrease in the spacing between the NCs and a dramatic loss of superlattice order upon EDT treatment. Measurements were taken in air. (b,c) Plan-view SEM images of (b) an untreated film and (c) a treated film. Untreated films have a peak-to-valley roughness of ±75 nm. Scale bars = 1 μm.

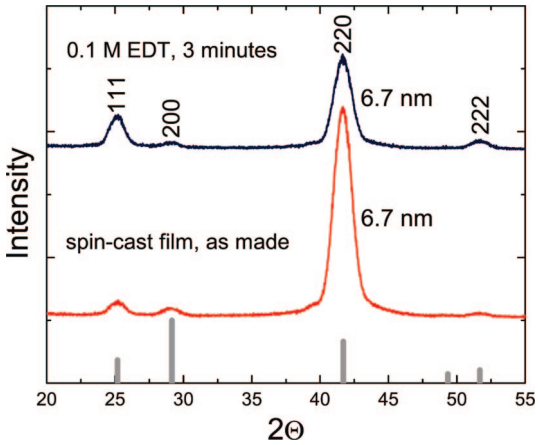

Figure 3. WAXS patterns of a spin-cast PbSe NC film before and after EDT treatment. Peaks index to rock-salt PbSe. The diameter of these NCs was determined to be 6.7 nm using the Scherrer equation for spherical particles. Measurements were made in air. A standard PbSe powder diffraction pattern is shown at the bottom.

istic of the isolated nanocrystals, to a dull gray. In principle, the red-shift and the enhanced absorbance could arise from changes in (i) the physical or the "electronic" size[35] of the NCs, (ii) the effective dielectric constant at the surface of the NCs, (iii) radiative electronic coupling between NCs, and (iv) the degree of wavefunction overlap between NCs (*i.e.*, nonradiative electronic coupling).[36] The first mechanism is ruled out by our X-ray diffraction data (Figure 3) and by absorption spectra showing that no red-shift occurs when oleic acid is replaced by octadecanethiol on the surface of the NCs in solution. To estimate the impact of the second and third mechanisms, we calculated changes in oscillator strength and dipole–induced dipole coupling due to loss of oleate and densification of the NC film (see Supporting Information). Using reasonable assumptions, we find that the enhanced absorbance is largely accounted for by an increase in the dielectric constant of the surrounding medium, whereas the red-shift is likely caused by a combination of strengthened dipole–induced dipole interactions and wavefunction delocalization, which is consistent with the large increase in DC conductivity upon EDT treatment (see below).

LbL NC Films. Whereas spin-coating yields disordered PbSe NC superlattices, LbL dip-coating produces glassy nanocrystal solids with little translational or crystallographic order evident by SEM or X-ray scattering. The NCs pack irregularly in the LbL films and form only small ordered domains (Figure 6a). The absence of significant peaks in SAXS patterns confirms that little medium-range order exists (Figure 7). Furthermore, wide-angle scattering patterns of the LbL films resemble PbSe powder patterns, indicating that the NCs are crystallographically isotropic (Figure 7 inset). This is in contrast to the spin-cast films, which show strong 220 texture. WAXS shows that EDT exposure during the LbL process does not alter the NC size. In addition, the LbL films and the spin-cast films have comparable FTIR spectra (Figure S7).

The LbL films and spin-cast films also have similar absorption spectra. Spectra of LbL films and spin-cast films of comparable thickness are nearly identical in shape, although the red-shift of the first exciton in the LbL films is usually somewhat smaller (20–24 meV rather than 24–27 meV for the spin-cast films; Figure 8). The smaller red-shift may reflect the somewhat less ordered and less dense NC packing of the LbL films.

Electrical Measurements. Field-effect transistors (FETs) made from the LbL films and the spin-cast films treated with EDT behave identically, showing a dark conductivity of 5×10^{-5} S cm^{-1} and ambipolar gating (Figure 9). Interestingly, the source−drain current of these devices, I_D, exhibits dramatic time dependence after a change in gate voltage, V_G. For example, a positive step in gate voltage causes I_D of the device in Figure 9 to spike and then decay exponentially to near its zero-gate current with a characteristic time constant of 5–7 s. Some I_D overshoot also occurs. The I_D transients associated with negative steps in V_G are well characterized by two decay constants, 0.5–1.5 s and 9–13 s. If smaller steps in V_G are used, I_D decays more quickly and overshoots less strongly or not at all. Although the exact values of the time constants vary somewhat from device to device, the overall behavior was fully reproducible across 25 EDT-treated devices prepared by either method. In all cases, the steady-state drain currents are independent of V_G (that is, $I_{D(V_G = -30\ V)} \approx I_{D(V_G = 30\ V)} \approx I_{D(V_G = 0\ V)}$), as if the gate field is completely screened by mobile charges in the FET channel. The time dependence of I_D prevents us from determining accurate values for the mobility of carriers in these films. As a check on the FET substrates and setup, we tested FETs made from spin-coated poly(3-hexyl)thiophene (P3HT), a well-characterized hole-conducting polymer.[37,38] The P3HT FETs showed stable current switching with changes in V_G (Figure S9). This rules out the possibility that problems with the setup (*e.g.*, parasitic gate currents due to low-quality gate oxide) cause the current transients. Instead, the transients must result from trap charging and/or charge redistribution within the NC films or at the NC/oxide interface in response to steps in the applied gate field.

We modified the surface of the gate oxide in two ways in an effort to stop the I_D transients. First, the substrates were thoroughly dehydrated prior to NC deposition by heating them to 250 °C for 8 h in a glovebox. This procedure eliminates any surface-bound water layer[39] that may act to trap charge at the NC/oxide interface; such a layer is suspected of causing significant I_D hysteresis in carbon nanotube FETs and ZnO nanowire FETs.[40–43] However, the use of dehydrated substrates had no effect on the I_D transients of our PbSe NC FETs. Second, the substrates were treated with hexamethyldisilazane (HMDS) prior to NC deposition by ex-

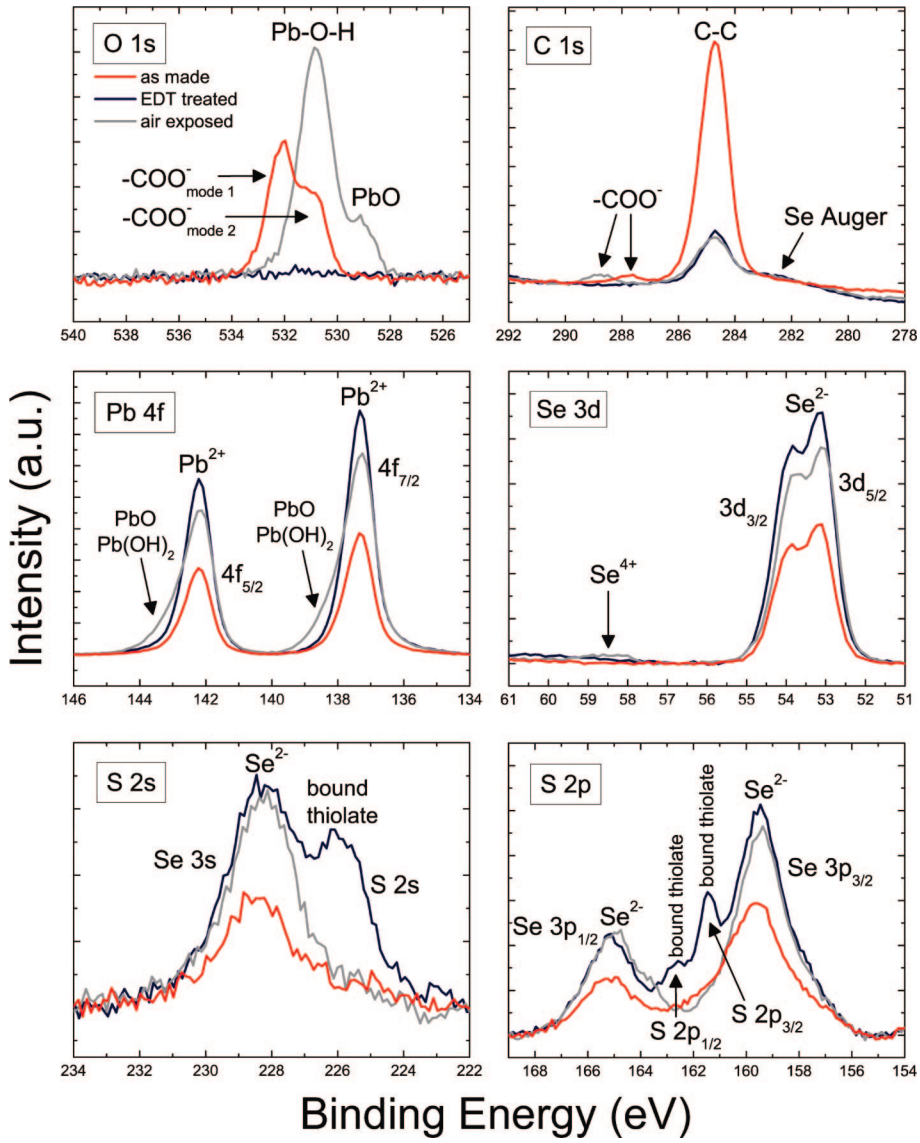

Figure 4. XPS analysis of untreated (red), EDT-treated (blue), and EDT-treated, air-exposed PbSe NC films (gray). Untreated films were measured without exposure to air. EDT-treated films were treated in 0.1 M EDT for several seconds and measured without exposure to air. Air-exposed films were treated in EDT and then exposed to air for 5 min. Untreated films show oxygen peaks at 532.1 and 530.8 eV, assigned to carboxylate oxygen atoms in two different surface-binding modes. The small carbon peak at 287.8 eV in the spectrum of the untreated film is assigned to the carboxylate ($-COO^-$) of the adsorbed oleate. The simultaneous disappearance of oxygen, reduction of carbon, and enhancement of lead and selenium on EDT-treated films is consistent with removal of the oleate ligand shell. Moreover, EDT-treated films show increased sulfur 2s and 2p signals, indicating that EDT adsorbs to the nanocrystals. Exposure of EDT-treated films to air for several minutes results in the appearance of a large amount of oxygen, small decreases in the lead and selenium signals, and loss of surface sulfur (see the section on film oxidation in the text). Oxygen peaks at 530.8 and 529.0 eV and the Pb shoulder at high binding energy are indicative of $Pb(OH)_2$ and PbO_x. A small amount of Se^{4+} is also present, probably as SeO_3^{2-} or SeO_2.

posing them to HMDS vapor or liquid at 130 °C for 2 h in a closed vessel. This procedure replaces the polar silanol-terminated SiO_2 surface with a hydrophobic trimethylsilyl-terminated surface,[44] which should reduce the density of charge traps, such as silanol groups (≡SiOH), at the silicon oxide surface. An increase in the contact angle of deionized water from 45 ± 5° to 83 ± 7° confirmed the efficacy of the HMDS procedure,[45] yet using HMDS-treated substrates also did not affect the I_D transients of the PbSe FETs.

We tentatively conclude, on the basis of the totality of the gate screening and the ineffectiveness of modifications to the surface of the gate oxide, that the I_D transients are caused by screening of the gate voltage by charges either injected into the SiO_2 itself or trapped on the layer of NCs immediately adjacent to the oxide surface. Other scenarios, such as charge trapping in the bulk of the NC film, would screen only part of the field and probably cannot explain our observations.

The PbSe NC FETs were also measured while illuminated by a broadband tungsten lamp in order to mimic solar cell operating conditions. At a light intensity of 300 mW cm^{-2}, the films become 30–60 times more conductive and switch from ambipolar to *p*-type behav-

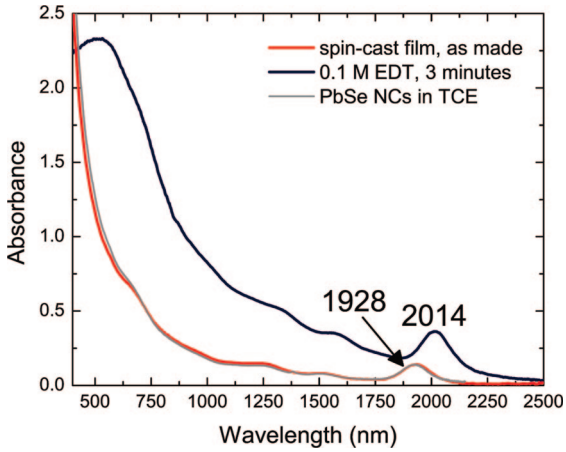

Figure 5. Optical absorption spectra of a spin-cast film before and after EDT treatment. Spectra were acquired in an inert atmosphere using an integrating sphere. A spectrum of the nanocrystals in tetrachloroethylene solution is also shown. Accurate measurements require that the samples be protected from air because the EDT-treated films oxidize in air within minutes (see Figure 12). The full width at half-maximum of the first exciton is 44 meV in each case.

ior, with $I_{ON}/I_{OFF} \approx 8$ (Figure 10). In addition, the time constants for I_D decay shorten to <1 s for both positive and negative steps in V_G, reflecting the larger number of free carriers available to fill traps within the illuminated films.

Oxidation of the NC Films. EDT-treated films, whether spin-cast or dip-coated, rapidly oxidize when exposed to air because the NC surfaces are not well protected by

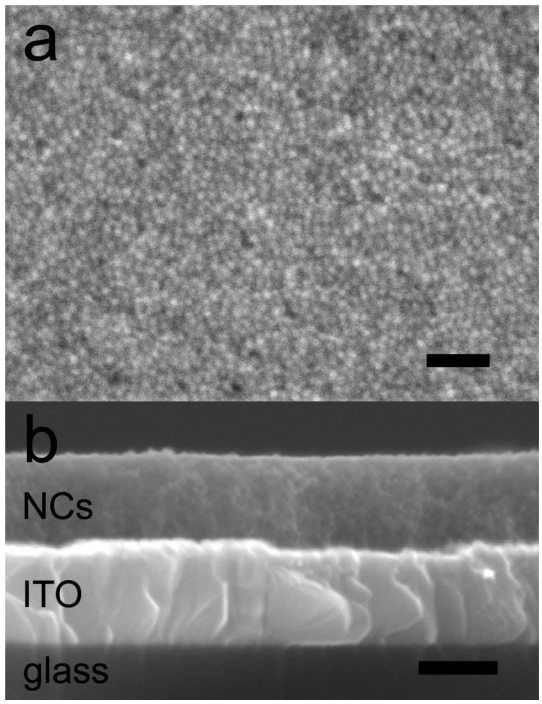

Figure 6. SEM images of PbSe NC films prepared by layer-by-layer dip-coating onto ITO substrates. (a) Plan view. Scale bar = 50 nm. (b) Cross section. Scale bar = 100 nm. All the LbL films studied in this paper were produced using 10–20 dip-coating cycles. See Figure S8 for a large-area SEM view of a typical film.

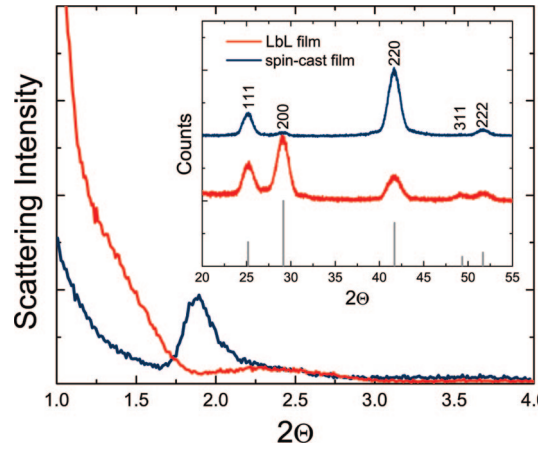

Figure 7. SAXS patterns of a typical LbL film and a spin-cast film treated with EDT. The inset displays the WAXS patterns. A standard PbSe powder diffraction pattern is shown at the bottom.

adsorbed EDT. Brief exposure to air results in the elimination of EDT from the film surface, as evident in both the reduction of C−H stretch intensity in FTIR spectra (Figure 1) and the loss of sulfur signal in XP spectra (Figure 4). We speculate that the EDT surface complex is hydrolyzed in air *via* the reaction shown in Scheme 1, illustrated here with EDT bound in a bidentate configuration to a single NC.

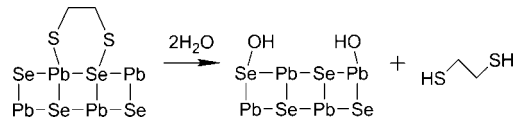

Scheme 1. Hydrolysis of adsorbed ethanedithiolate on PbSe {100}.

FTIR spectra indeed show the appearance of a small O−H band after air exposure, but it seems too weak for EDT loss to occur exclusively by Scheme 1. A second possibility is that adsorbed EDT is oxidized and lost

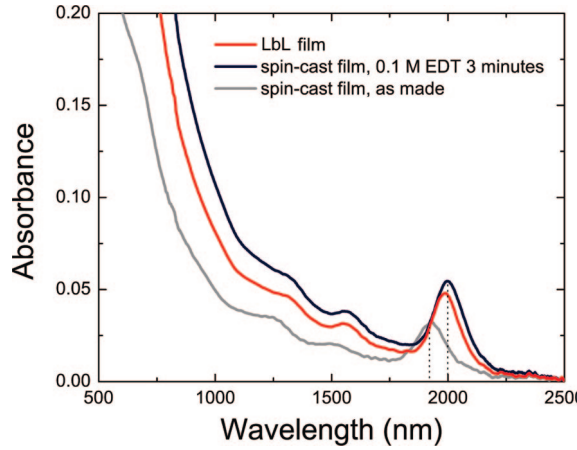

Figure 8. Optical absorption spectra of a typical LbL PbSe NC film and a spin-cast film before and after EDT treatment, acquired with an integrating sphere in an air-free cell. The LbL film and EDT-treated spin-cast film are ~110 nm thick. The LbL film shows an intermediate red-shift (to 1986 nm, *versus* 2000 nm for the spin-cast film) and otherwise resembles the EDT-treated spin-cast film.

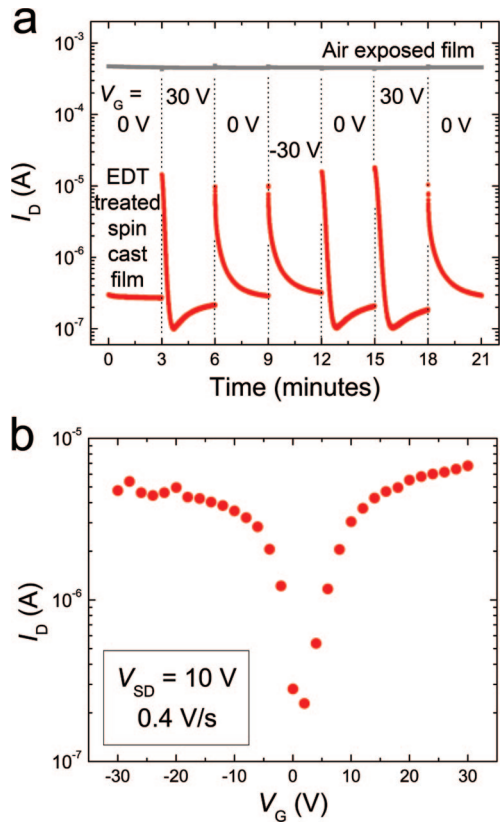

Figure 9. Behavior of spin-cast PbSe NC FETs treated with EDT. (a) Time dependence of I_D as a function of V_G in the dark. The gate voltage was cycled between −30 and +30 V using 30 V steps every 3 min. V_{DS} = 10 V. Also shown are data for the same FET after it was exposed to air for 5 min (see text). Similar behavior is seen with 1 and 10 V steps in V_G. (b) Transfer characteristics of the EDT-treated FET, showing ambipolar conduction (L = 23 μm, W = 2100 μm, t = 75 nm). See Figure S10 for SEM images of this device.

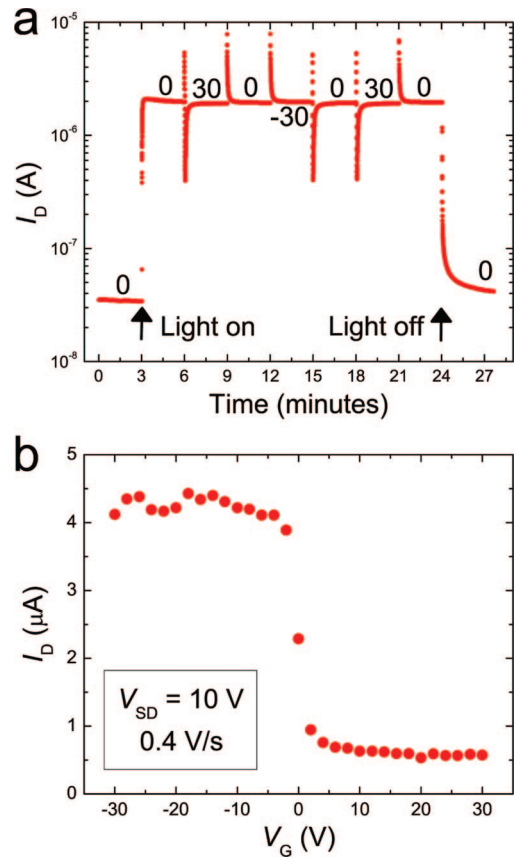

Figure 10. Behavior of a PbSe NC FET under 300 mW cm^{-2} illumination by a tungsten lamp. (a) Time trace using 30 V gate voltage steps. (b) Transfer characteristics of the device in the light (L = 23 μm, W = 2100 μm, t = 60 ± 10 nm).

as a cyclic disulfide rather than the dithiol. XPS analysis of films exposed to air for 5 min reveals that oxygen is bound primarily to lead, probably as a mixture of lead oxides and hydroxides (Figure 4 and Table 1). Small amounts of SeO_3^{2-} (or SeO_2) and a carboxylate species also appear on the surface. The presence of adsorbed water, molecular oxygen, and other species cannot be ruled out by these XPS data. Our results are in agreement with past studies of PbSe surface oxidation.[46,47]

XPS depth profiles reveal that the interior of the NC films is significantly different from their outer surface (Figure 11). While the surface of films exposed to air for 5 min is devoid of sulfur, their interior contains 1.7 ± 0.8 atom % sulfur, about half of the sulfur XP intensity measured for films freshly treated with EDT (see Figure S6). Short air exposures therefore do not remove all of the EDT adsorbed *within* the films. Oxygen is found within the air-exposed films at a concentration of 2.7 ± 1.6 atom %, which is substantially higher than the 0.55 ± 0.4 atom % oxygen in fresh EDT-treated films but 6 times lower than at the surface of air-exposed films. An oxygen-rich surface layer is to be expected on the basis of simple gas diffusion considerations. Nevertheless, the oxygen concentration at depth is probably underestimated because of preferential sputtering of oxygen by the ion beam during depth profiling. Similar considerations apply to carbon (and maybe sulfur): one must be cautious in quantifying carbon in depth profiles because of the tendency of organic adsorbates to be damaged and removed from the surface by the sputter beam, resulting in erroneously low carbon concentrations. Note that the sulfur loading in the fresh EDT-treated films may also be underestimated by the depth profiles. With this caveat in mind, we interpret the null carbon signal within the film in Figure 11 to mean only that air exposure reduces the carbon content of the EDT-treated films (which themselves show only 1.7 ± 0.9 atom % carbon, almost certainly an underestimate). Taken as a whole, the XPS data indicate that air exposure partially removes sulfur and carbon while adding oxygen, consistent with substantial EDT loss and surface oxidation throughout the air-exposed films.

Oxidation also has a major impact on the optical and electrical properties of the films. Air exposure results in a marked blue-shift and weakening of the first excitonic transition in absorption spectra, indicating a reduction in inter-NC coupling and NC size (Figure 12a).

TABLE 1. XPS Surface Composition (Atom %) of the PbSe NC Films Before Depth Profiling

film	C 1s	O 1s	S 2s	Pb 4f	Se 3d
as-made	70.6	7.8	0	11.1	10.5
EDT-treated	27.3	0.9	5.0	35.4	31.4
air-exposed	27.0	18.3	0	31.0	23.7

Untreated films do not show a blue-shift on this time scale. Furthermore, air-exposed films become 1500–5000 times more conductive and switch from ambipolar to *p*-type behavior, with $I_{ON}/I_{OFF} \approx 1$ (Figure 12b). We find this large increase in conductivity upon air exposure detrimental to the performance of solar cells employing these films.

CONCLUSIONS

Layer-by-layer dip-coating using 1,2-ethanedithiol produces uniform and conductive PbSe nanocrystal films with excellent control of the film thickness over large areas. Compared to spin-coating and drop-casting, LbL assembly is tedious but avoids the formation of cracks and other film defects that frustrate the reproducible construction of solar cells from NC solids. EDT exchanges quantitatively for oleate, producing FETs that are moderately conductive and ambipolar in the dark, becoming *p*-type and 30–60 times more conductive under 300 mW cm^{-2} broadband illumination. We find little difference in the electrical behavior of films made by LbL and by spin-coating, despite the greater degree of crystallinity and texturing in the spin-cast NC films. Complete compensation of V_G in the PbSe NC FETs is probably caused by screening of the gate voltage by charges either injected into the SiO_2 itself or trapped on the layer of NCs adjacent to the oxide surface. These time-dependent drain currents preclude the determination of the carrier mobilities of these films. EDT-treated PbSe NC films oxidize rapidly in air to yield, after short air exposures, highly conductive *p*-type solids. It is likely that longer air exposures convert the films to insulating PbSe/PbO_{1-x} or PbSe/$PbSeO_3$ core–shell NC solids.

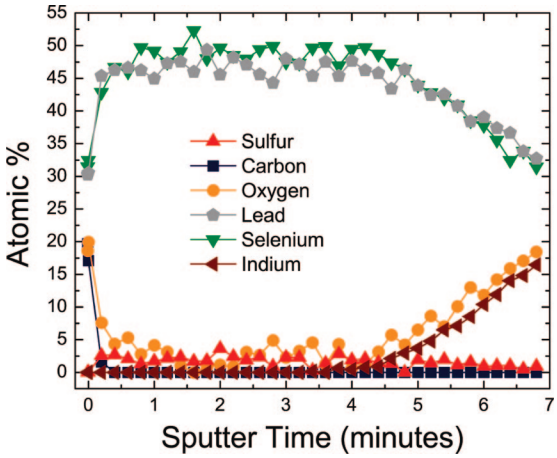

Figure 11. XPS depth profile of a 70-nm-thick LbL NC film on ITO exposed to air for 5 min. Sputter profiling was performed using a 3 keV Ar^+ beam at a current density of 20 μA cm^{-2}.

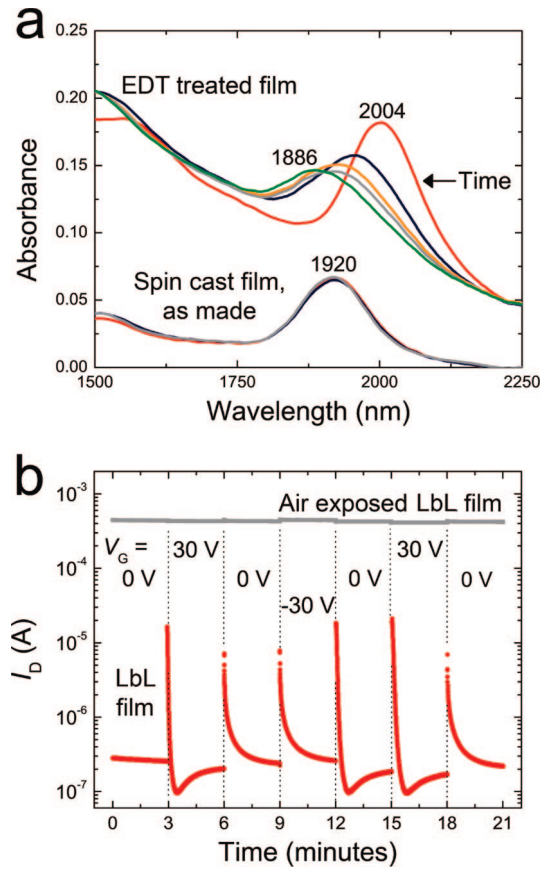

Figure 12. Oxidation of PbSe NC films. (a) Optical absorption spectra of an untreated spin-cast film and a treated spin-cast film as a function of time in air. Samples were first measured in an air-free sample cell and then exposed to air. Untreated, oleate-capped films show no change after 25 min in air. In contrast, the first exciton peak of EDT-treated films progressively blue-shifts and weakens with time. Plots of the treated film correspond to 0, 2, 14, 26, and 65 min of air exposure. (b) Time dependence of the source−drain current of an LbL PbSe FET as a function of gate voltage before and after 5 min of air exposure. Air-exposed FETs become very conductive and *p*-type, with $I_{on}/I_{off} \approx 1$. Note the similarity to the spin-cast film in Figure 9a (L = 23 μm, W = 2100 μm, t = 60 ± 10 nm).

There is insufficient evidence to claim, as others recently have,[48] that EDT acts to covalently interlink the nanocrystals in the solid. Dithiols are widely reported to readily cross-link noble metal[49–52] and metal chalcogenide NCs.[35,53–56] In the case of our EDT-treated films, however, the absence of S−H FTIR signal cannot be used to differentiate between bidentate bonding on single NCs and bridging between NCs. If EDT does act as a linker, its direct role in enhancing the electrical conductivity of NC films is dubious because it lacks conjugation, which is vital for through-bond conduction.[55,57] In fact, we have fabricated NC solar cells exhibiting short-circuit currents of 18 mA cm^{-2} from LbL PbSe films fabricated using methylamine, a molecule that cannot bridge NCs. This shows that (i) the LbL process

described here is a general method for producing high-quality NC films for device applications and (ii) the main function of the EDT treatment is probably to decrease the inter-NC separation by removing oleate, rather than to provide through-bond conduction between nanocrystals.

METHODS

Materials. Lead oxide (99.999%), selenium (99.99%), oleic acid (technical grade, 90%), 1-octadecene (ODE, 90%), diphenylphosphine (DPP, 98%), tetrachloroethylene (TCE, 99.9+%), and anhydrous methanol, acetone, hexane, octane, and acetonitrile were purchased from Aldrich and used as received. Trioctylphosphine (TOP, technical grade, >90%) and 1,2-ethanedithiol (EDT, >98%) were acquired from Fluka.

PbSe Nanocrystal Synthesis. Standard air-free techniques were employed throughout. In a typical synthesis, 0.22 g of PbO was dissolved in a mixture of 0.73 g of oleic acid and 10 g of ODE at 150 °C to yield a clear solution. A mixture of 3 mL of 1 M TOP-Se and 28 mg of DPP was swiftly injected into the solution once its temperature reached 180 °C, and the temperature was reduced to 155–160 °C to allow the NCs to grow to the desired size. DPP, which enhances the NC yield,[27] was used in some but not all of the syntheses. The solution was then cooled, 10 mL of hexane was added, and the NCs were extracted with methanol and precipitated with acetone. Finally, the NCs were washed three times with acetone and stored as a powder. The synthesis results in monodisperse, oleate-capped PbSe nanocrystals that have been characterized in detail elsewhere.[28] We used several NC samples in this study, each with an average NC diameter in the range of 6–8 nm.

Preparation of NC Films by Spin-Coating. All processing occurred in a nitrogen glovebox. PbSe NC films were made by spin-coating ~100 μL of a 380 mg mL^{-1} NC solution in octane onto various substrates, such as 1-in. sapphire windows, double-side-polished intrinsic silicon substrates, glass coated with indium tin oxide (ITO), or degenerate silicon coated with a 110-nm-thick thermal oxide. As-made films were typically 450 nm thick with a peak-to-valley roughness of ±75 nm as measured in SEM cross sections. To treat films with EDT, they were immersed in 0.1 M EDT solutions in anhydrous acetonitrile for 3 min and blown dry in a stream of nitrogen.

Preparation of NC Films by Layer-by-Layer Assembly. All processing occurred in a helium glovebox. Substrates were dipped by hand into a dilute solution of NCs in hexane (~5 mg mL^{-1}) and then slowly removed from the solution at a velocity of ~0.5 cm s^{-1}. Once dry, substrates were dipped into a beaker containing 0.1 M EDT in anhydrous acetonitrile for several seconds, quickly removed, and allowed to dry before repeating the dipping sequence. Substrates were rotated 90° after each treatment in EDT to ensure film uniformity. Careful dip-coating results in the addition of less than a monolayer of NCs with each step, yielding smooth films across several square centimeters. Solutions of higher NC concentration tend to deposit thicker NC layers per cycle.

Film Characterization. Fourier transform infrared data were taken on a Nicolet 510 FTIR spectrometer in transmission mode. SAXS and WAXS measurements were carried out with a Scintag X1 diffractometer (Cu Kα radiation). A JEOL JSM-7000F field emission scanning electron microscope was used to image the films. Optical absorption data were acquired with a Shimadzu UV-3600 spectrophotometer equipped with an integrating sphere. For XPS analysis, samples were transferred in an inert atmosphere from the fabrication glovebox to another glovebox integrated with the ultra-high-vacuum tools, thus avoiding any exposure to air. Films were analyzed "as-prepared" and without any sputter cleaning. Data were obtained on a Physical Electronics 5600 photoemission system using monochromatic Al Kα radiation and a pass energy of 29 eV. The films were found to charge slightly during analysis, so spectra were aligned by placing the Pb $4f_{7/2}$ peak at the lowest observed binding energy of 137.3 eV (seen on the EDT-treated films).

For electrical studies, PbSe NC films were deposited onto degenerately doped silicon substrates coated with a 110-nm-thick thermal SiO_2 gate oxide. Source and drain electrodes (5 nm Ti/35 nm Au) spaced 10–50 μm apart were patterned onto the SiO_2 surface before NC deposition. When samples were made by spin-coating, two rounds of NC deposition and EDT treatment were used to prepare 75-nm-thick films free of through-film cracks. The portion of each NC film covering the contact pads and touching the underlying silicon substrate (the gate electrode) was then removed with a swab. Field-effect measurements were performed in a glovebox using a Keithley 236 source-measure unit (source−drain) and a Keithley 230 programmable voltage source (gate) driven by Labview software. The noise limit of the setup was ~10 pA. The resistance of the untreated, oleate-capped NC films was always too large to measure with this equipment.

Acknowledgment. We thank S. Shaheen and group for use of the fabrication glovebox, L. Gedvilas for assistance with FTIR, M. Page for wafer preparation, J. Chandler for SEM support, and P. Parilla for a kind introduction to SAXS measurements. Funding is provided by the U.S. Department of Energy, Office of Basic Energy Sciences, Division of Chemical Sciences, Biosciences and Geosciences.

Supporting Information Available: Calculations of dielectric effects on film optical properties, reaction schemes for oleate removal by EDT, FTIR data on the LbL films and neat EDT/ethanethiol, XPS depth profiles, SEM imaging of a PbSe NC FET, and the performance of P3HT FETs. This material is available free of charge *via* the Internet at http://pubs.acs.org.

REFERENCES AND NOTES

1. Ridley, B. A.; Nivi, B.; Jacobson, J. M. All-Inorganic Field Effect Transistors Fabricated by Printing. *Science* **1999**, *286*, 746–749.
2. Morgan, N. Y.; Leatherdale, C. A.; Drndic, M.; Jarosz, M. V.; Kastner, M. A.; Bawendi, M. Electronic Transport in Films of Colloidal CdSe Nanocrystals. *Phys. Rev. B* **2002**, *66*, 075339.
3. Yu, D.; Wang, C. J.; Guyot-Sionnest, P. n-type Conducting CdSe Nanocrystal Solids. *Science* **2003**, *300*, 1277–1280.
4. Talapin, D. V.; Murray, C. B. PbSe Nanocrystal Solids for n- and p-Channel Thin Film Field-Effect Transistors. *Science* **2005**, *310*, 86–89.
5. Porter, V. J.; Mentzel, T.; Charpentier, S.; Kastner, M. A.; Bawendi, M. G. Temperature-, Gate-, and Photoinduced Conductance of Close-Packed CdTe Nanocrystal Films. *Phys. Rev. B* **2006**, *73*, 155303.
6. Urban, J. J.; Talapin, D. V.; Shevchenko, E. V.; Kagan, C. R.; Murray, C. B. Synergism in Binary Nanocrystal Superlattices Leads to Enhanced p-type Conductivity in Self-Assembled PbTe/Ag_2Te Thin Films. *Nat. Mater.* **2007**, *6*, 115–121.
7. Kim, H.; Cho, K.; Kim, D. W.; Lee, H. R.; Kim, S. Bottom- and Top-Gate Field-Effect Thin-Film Transistors with p Channels of Sintered HgTe Nanocrystals. *Appl. Phys. Lett.* **2006**, *89*, 173107.
8. Ginger, D. S.; Greenham, N. C. Charge Injection and Transport in Films of CdSe Nanocrystals. *J. Appl. Phys.* **2000**, *87*, 1361–1368.
9. Jarosz, M. V.; Porter, V. J.; Fisher, B. R.; Kastner, M. A.; Bawendi, M. G. Photoconductivity Studies of Treated CdSe Quantum Dot Films Exhibiting Increased Exciton Ionization Efficiency. *Phys. Rev. B* **2004**, *70*, 195327.
10. Konstantatos, G.; Howard, I.; Fischer, A.; Hoogland, S.; Clifford, J.; Klem, E.; Levina, L.; Sargent, E. H. Ultrasensitive Solution-Cast Quantum Dot Photodetectors. *Nature* **2006**, *442*, 180–183.

11. Oertel, D. C.; Bawendi, M. G.; Arango, A. C.; Bulovic, V. Photodetectors Based on Treated CdSe Quantum-Dot Films. *Appl. Phys. Lett.* **2005**, *87*, 213505.
12. Artemyev, M. V.; Sperling, V.; Woggon, U. Electroluminescence in Thin Solid Films of Closely Packed CdS Nanocrystals. *J. Appl. Phys.* **1997**, *81*, 6975–6977.
13. Bertoni, C.; Gallardo, D.; Dunn, S.; Gaponik, N.; Eychmuller, A. Fabrication and Characterization of Red-Emitting Electroluminescent Devices Based on Thiol-Stabilized Semiconductor Nanocrystals. *Appl. Phys. Lett.* **2007**, *90*, 034107.
14. Coe, S.; Woo, W. K.; Bawendi, M.; Bulovic, V. Electroluminescence from Single Monolayers of Nanocrystals in Molecular Organic Devices. *Nature* **2002**, *420*, 800–803.
15. Colvin, V. L.; Schlamp, M. C.; Alivisatos, A. P. Light Emitting Diodes made from Cadmium Selenide Nanocrystals and a Semiconducting Polymer. *Nature* **1994**, *370*, 354–357.
16. Gao, M. Y.; Lesser, C.; Kirstein, S.; Mohwald, H.; Rogach, A. L.; Weller, H. Electroluminescence of Different Colors from Polycation/CdTe Nanocrystal Self-Assembled Films. *J. Appl. Phys.* **2000**, *87*, 2297–2302.
17. Redl, F. X.; Cho, K. S.; Murray, C. B.; O'Brien, S. Three-Dimensional Binary Superlattices of Magnetic Nanocrystals and Semiconductor Quantum Dots. *Nature* **2003**, *423*, 968–971.
18. Shevchenko, E. V.; Talapin, D. V.; Kotov, N. A.; O'Brien, S.; Murray, C. B. Structural Diversity in Binary Nanoparticle Superlattices. *Nature* **2006**, *439*, 55–59.
19. Shevchenko, E. V.; Talapin, D. V.; Murray, C. B.; O'Brien, S. Structural Characterization of Self-Assembled Multifunctional Binary Nanoparticle Superlattices. *J. Am. Chem. Soc.* **2006**, *128*, 3620–3637.
20. Gur, I.; Fromer, N. A.; Geier, M. L.; Alivisatos, A. P. Air-Stable All-Inorganic Nanocrystal Solar Cells Processed from Solution. *Science* **2005**, *310*, 462–465.
21. Nozik, A. J. Quantum Dot Solar Cells. *Phys. E* **2002**, *14*, 115–120.
22. Ellingson, R. J.; Beard, M. C.; Johnson, J. C.; Yu, P. R.; Micic, O. I.; Nozik, A. J.; Shabaev, A.; Efros, A. L. Highly Efficient Multiple Exciton Generation in Colloidal PbSe and PbS Quantum Dots. *Nano Lett.* **2005**, *5*, 865–871.
23. Schaller, R. D.; Klimov, V. I. High Efficiency Carrier Multiplication in PbSe Nanocrystals: Implications for Solar Energy Conversion. *Phys. Rev. Lett.* **2004**, *92*, 186601.
24. Luther, J. M.; Beard, M. C.; Song, Q.; Law, M.; Ellingson, R. J.; Nozik, A. J. Multiple Exciton Generation in Films of Electronically Coupled PbSe Quantum Dots. *Nano Lett.* **2007**, *7*, 1779–1784.
25. Hanna, M. C.; Nozik, A. J. Solar Conversion Efficiency of Photovoltaic and Photoelectrolysis Cells with Carrier Multiplication Absorbers. *J. Appl. Phys.* **2006**, *100*, 074510.
26. Luther, J. M.; Law, M.; Song, Q.; Beard, M. C.; Ellingson, R. J.; Nozik, A. J. Manuscript in preparation.
27. Steckel, J. S.; Yen, B. K. H.; Oertel, D. C.; Bawendi, M. G. On the Mechanism of Lead Chalcogenide Nanocrystal Formation. *J. Am. Chem. Soc.* **2006**, *128*, 13032–13033.
28. Murphy, J. E.; Beard, M. C.; Norman, A. G.; Ahrenkiel, S. P.; Johnson, J. C.; Yu, P. R.; Micic, O. I.; Ellingson, R. J.; Nozik, A. J. PbTe Colloidal Nanocrystals: Synthesis, Characterization, and Multiple Exciton Generation. *J. Am. Chem. Soc.* **2006**, *128*, 3241–3247.
29. Substantially lower EDT concentrations are equally effective, while pure acetonitrile has no effect on the films. See Figure S4, Supporting Information.
30. Wu, N. Q.; Fu, L.; Su, M.; Aslam, M.; Wong, K. C.; Dravid, V. P. Interaction of Fatty Acid Monolayers with Cobalt Nanoparticles. *Nano Lett.* **2004**, *4*, 383–386.
31. Roe, C. L.; Schulz, K. H. Reaction of 1,2-ethanedithiol on Clean, Sulfur-Modified, and Carbon-Modified Mo(110) Surfaces. *J. Vac. Sci. Technol., A* **1998**, *16*, 1066–1072.
32. Joo, S. W.; Han, S. W.; Kim, K. Multilayer Formation of 1,2-ethanedithiol on Gold: Surface-Enhanced Raman Scattering and Ellipsometry Study. *Langmuir* **2000**, *16*, 5391–5396.
33. Castner, D. G.; Hinds, K.; Grainger, D. W. X-ray Photoelectron Spectroscopy Sulfur 2p Study of Organic Thiol and Disulfide Binding Interactions with Gold Surfaces. *Langmuir* **1996**, *12*, 5083–5086.
34. Remacle, F. On Electronic Properties of Assemblies of Quantum Nanodots. *J. Phys. Chem. A* **2000**, *104*, 4739–4747.
35. Koole, R.; Luigjes, B.; Tachiya, M.; Pool, R.; Vlugt, T. J. H.; Donega, C. D. M.; Meijerink, A.; Vanmaekelbergh, D. Differences in Cross-Link Chemistry Between Rigid and Flexible Dithiol Molecules Revealed by Optical Studies of CdTe Quantum Dots. *J. Phys. Chem. C* **2007**, *111*, 11208–11215.
36. Schedelbeck, G.; Wegscheider, W.; Bichler, M.; Abstreiter, G. Coupled Quantum Dots Fabricated by Cleaved Edge Overgrowth: From Artificial Atoms to Molecules. *Science* **1997**, *278*, 1792–1795.
37. Sirringhaus, H.; Brown, P. J.; Friend, R. H.; Nielsen, M. M.; Bechgaard, K.; Langeveld-Voss, B. M. W.; Spiering, A. J. H.; Janssen, R. A. J.; Meijer, E. W.; Herwig, P.; de Leeuw, D. M. Two-Dimensional Charge Transport in Self-Organized, High-Mobility Conjugated Polymers. *Nature* **1999**, *401*, 685–688.
38. Kline, R. J.; McGehee, M. D.; Kadnikova, E. N.; Liu, J. S.; Frechet, J. M. J. Controlling the Field-Effect Mobility of Regioregular Polythiophene by Changing the Molecular Weight. *Adv. Mater.* **2003**, *15*, 1519–1522.
39. Zhuravlev, L. T. The Surface Chemistry of Amorphous Silica. Zhuravlev Model. *Colloids Surf., A* **2000**, *173*, 1–38.
40. Kim, W.; Javey, A.; Vermesh, O.; Wang, O.; Li, Y. M.; Dai, H. J. Hysteresis Caused by Water Molecules in Carbon Nanotube Field-Effect Transistors. *Nano Lett.* **2003**, *3*, 193–198.
41. Vijayaraghavan, A.; Kar, S.; Soldano, C.; Talapatra, S.; Nalamasu, O.; Ajayan, P. M. Charge-Injection-Induced Dynamic Screening and Origin of Hysteresis in Field-Modulated Transport in Single-Wall Carbon Nanotubes. *Appl. Phys. Lett.* **2006**, *89*, 162108.
42. Lee, J. S.; Ryu, S.; Yoo, K.; Choi, I. S.; Yun, W. S.; Kim, J. Origin of Gate Hysteresis in Carbon Nanotube Field-Effect Transistors. *J. Phys. Chem. C* **2007**, *111*, 12504–12507.
43. Goldberger, J.; Sirbuly, D. J.; Law, M.; Yang, P. ZnO Nanowire Transistors. *J Phys. Chem. B* **2005**, *109*, 9–14.
44. Hertl, W.; Hair, M. L. Reaction of Hexamethyldisilazane with Silica. *J. Phys. Chem.* **1971**, *75*, 2181–2185.
45. Lim, S. C.; Kim, S. H.; Lee, J. H.; Kim, M. K.; Kim, D. J.; Zyung, T. Surface-Treatment Effects on Organic Thin-Film Transistors. *Synth. Met.* **2005**, *148*, 75–79.
46. Gautier, C.; Cambon-Muller, M.; Averous, M. Study of PbSe Layer Oxidation and Oxide Dissolution. *Appl. Surf. Sci.* **1999**, *141*, 157–163.
47. Sarkar, S. K.; Kababya, S.; Vega, S.; Cohen, H.; Woicik, J. C.; Frenkel, A. I.; Hodes, G. Effects of Solution pH and Surface Chemistry on the Postdeposition Growth of Chemical Bath Deposited PbSe Nanocrystalline Films. *Chem. Mater.* **2007**, *19*, 879–888.
48. Klem, E. J. D.; MacNeil, D. D.; Cyr, P. W.; Levina, L.; Sargent, E. H. Efficient Solution-Processed Infrared Photovoltaic Cells: Planarized All-Inorganic Bulk Heterojunction Devices via Inter-Quantum-Dot Bridging during Growth from Solution. *Appl. Phys. Lett.* **2007**, *90*, 183113.
49. Leibowitz, F. L.; Zheng, W. X.; Maye, M. M.; Zhong, C. J. Structures and Properties of Nanoparticle Thin Films Formed via a One-Step Exchange-Cross-Linking−Precipitation Route. *Anal. Chem.* **1999**, *71*, 5076–5083.
50. Ahonen, P.; Laaksonen, T.; Nykanen, A.; Ruokolainen, J.; Kontturi, K. Formation of Stable Ag-Nanoparticle Aggregates Induced by Dithiol Cross-Linking. *J. Phys. Chem. B* **2006**, *110*, 12954–12958.
51. Brust, M.; Bethell, D.; Schiffrin, D. J.; Kiely, C. J. Novel Gold-Dithiol Nano-Networks with Nonmetallic Electronic Properties. *Adv. Mater.* **1995**, *7*, 795–797.

52. Zabet-Khosousi, A.; Trudeau, P. E.; Suganuma, Y.; Dhirani, A. A.; Statt, B. Metal to Insulator Transition in Films of Molecularly Linked Gold Nanoparticles. *Phys. Rev. Lett.* **2006**, *96*, 156403.
53. Koole, R.; Liljeroth, P.; Donega, C. D.; Vanmaekelbergh, D.; Meijerink, A. Electronic Coupling and Exciton Energy Transfer in CdTe Quantum-Dot Molecules. *J. Am. Chem. Soc.* **2006**, *128*, 10436–10441.
54. Pacifico, J.; Jasieniak, J.; Gomez, D. E.; Mulvaney, P. Tunable 3-D Arrays of Quantum Dots: Synthesis and Luminescence Properties. *Small* **2006**, *2*, 199–203.
55. Ouyang, M.; Awschalom, D. D. Coherent Spin Transfer between Molecularly Bridged Quantum Dots. *Science* **2003**, *301*, 1074–1078.
56. Torimoto, T.; Tsumura, N.; Nakamura, H.; Kuwabata, S.; Sakata, T.; Mori, H.; Yoneyama, H. Photoelectrochemical Properties of Size-Quantized Semiconductor Photoelectrodes Prepared by Two-Dimensional Cross-Linking of Monodisperse CdS Nanoparticles. *Electrochim. Acta* **2000**, *45*, 3269–3276.
57. Schrier, J.; Whaley, K. B. Atomistic Theory of Coherent Spin Transfer between Molecularly Bridged Quantum Dots. *Phys. Rev. B* **2005**, *72*, 085320.